

The Effect of Nanoparticle Aggregation on the Radiative Properties of Plasmonic Nanofluid during Light-induced Vaporization Process

Yifan Zhang, Wei An*, Chang Zhao, Qingchun Dong
College of Mechanical Engineering, Tongji University, Shanghai, P.R. China

Abstract The light-induced vaporization process of plasmonic nanofluid plays an essential role in emerging efficient plasma-enhanced processes, ranging from solar energy harvesting to optofluidic control. In the current study, the effect of gold nanoparticle (AuNP) aggregation on the radiation properties during light-induced vaporization process has been investigated based on the finite element modeling (FEM). Specifically, the influence of the number and morphology of AuNP aggregates on the extinction cross section, albedo, and LSPR peak wavelength of particle-bubble complexes (P-B complexes) is studied. The results indicate that with the vaporization process of nanofluid, the radiative properties exhibit an obvious non-linear evolution law on the time scale and a periodic evolution pattern in the reciprocal cycle stages. The aggregation of AuNPs increases the peak extinction cross section. In the presence of nanobubble, whether the albedo of P-B complexes exceeds 0.5 depends on the relative magnitude of the extinction cross section of AuNP aggregates and nanobubble. After nanobubble dissipation, the aggregation of AuNPs increases the albedo of AuNP aggregates, although the albedo is still less than 0.5, showing a strong absorption of incident light. The aggregation of AuNPs causes a red-shift in the peak LSPR wavelength of AuNP aggregates, while the generation of nanobubble causes a blue-shift in the peak LSPR wavelength of AuNPs. In the presence of nanobubble, the change in the peak LSPR wavelength of P-B complexes depends on the competition between the red-shift effect of AuNPs aggregation and the blue-shift effect of nanobubble, but in general the red-shifting effect of AuNP aggregation is stronger than the blue-shifting effect of nanobubble. The increase in the number of AuNPs aggregation layers causes the blue-shifted LSPR peak wavelength of AuNP aggregates, the decreased peak extinction cross section, the increased LSPR peak width, and the potential for multiple extinction peaks.

Keywords: aggregation morphology, radiative properties, vaporization process, plasmonic nanofluid

1. Introduction

Recently, it was proven that steam might be produced with outstanding efficiency from liquids containing metallic nanoparticles (NPs) and illuminated by focused light [1, 2]. This process is of great significance for many plasmonic-enhanced applications, ranging from solar energy utilization [3], and optofluidic control [4] to biomedicine [5]. It is widely known that the interaction between NPs and visible light can excite localized surface plasmon resonance (LSPR). This phenomenon is characterized by intense absorption and scattering of light at the LSPR wavelength of the NP, thus effectively converting light energy into heat [6]. The intensively heated NPs under light illumination can be served as an effective local heat source at nanoscale to generate plasmonic nanobubbles (PNBs) around NPs [7]. Under continuous light illumination, these PNBs combine to generate larger PNBs, eventually achieving buoyancy, moving toward the liquid-air interface, and releasing the vapor [2]. Fig. 1 depicts the light-induced vaporization process of nanofluid.

The absorption of incident light energy by NPs, and the subsequent generation of photothermal and LSPR effect, transform NPs into “localized heat sources” with a high temperature in nanoscale and “charged particles” with time-varying enhanced electric fields (Fig. 1e) [1]. With the combination of the two effects mentioned above, PNBs will be formed around NPs when the temperature of the surrounding fluid reaches the spinodal temperature [8, 9]. After PNB generation, surface tension may lead to the formation of micro-convection around a PNB, which may attract NPs located within a certain distance of the PNB toward the PNB (Fig. 1b) [10]. Once the NPs come into contact with the PNB's surface, a balance between surface tension forces and pressure forces keeps the NPs on the PNB's surface, allowing NPs to move with PNBs without detaching [11]. PNBs may also fuse with other PNBs as they rise gradually under the combined effect of buoyancy forces and micro-convective (Fig. 1c). When the particle-bubble complexes (P-B complexes) move toward the liquid/air interface, the PNBs will overflow the fluid surface and release the vapor (Fig. 1d).

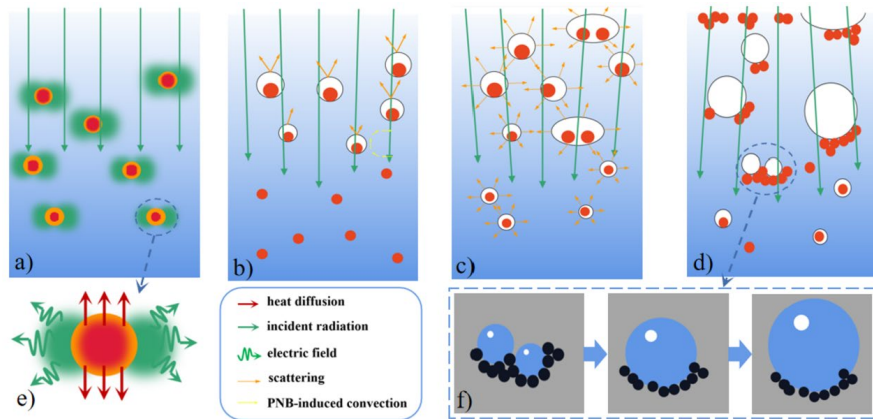


Fig. 1: Light-induced vaporization process of nanofluid. (a) Generation of the localized enhanced electric field and photothermal effect by the absorption of incident light energy by NPs. (b) Generation of PNBs and formation of scattering effect on the incident light. (c) Uplift and possible fusion of PNBs. (d) PNB-induced aggregation of NPs, and aggregation of NPs on the liquid surface after PNB dissipation. (e) Schematic diagram of temperature increase and generation of localized enhanced electric field. (f) Aggregation process of NPs during PNB growth and fusion.

Several researchers have investigated the nucleation and initial expansion of a PNB around a single AuNP and clustered AuNPs under continuous-wave and pulsed-laser excitation [12, 13], involving direct imaging of transient PNBs on the NP surface [14], measurements of the temporary decrease in the transmitted probe laser intensity [13], and the shift in the LSPR wavelength of NP [15]. During PNB generation, however, the time scale of the PNB events is at the nanosecond level, which demands a high temporal resolution of the detection instruments. Currently, only limited temporal resolution results can be obtained, causing early events in PNB dynamics to be obscured [16]. The simulation-based methods can offer a new perspective for obtaining the detailed evolution of radiation properties at different stages of the light-induced nanofluid vaporization process, since it is not constrained by experimental circumstances and instrument resolution. Katayama et al. [9] applied a model consisting of two concentric spheres (Au core and bubble shell) immersed in an aqueous medium for spectral simulations. In addition, Setoura et al. [17] computed the extinction spectra of a single AuNP immersed in water and surrounded by PNB of various sizes by considering the gradient change of the refractive index of the medium based on the Mie theory. According to the previous simulation results, after the formation of PNB, the peak wavelength of the scattering intensity of AuNP shows a noticeable blue shift, and the extinction intensity has a significant attenuation. The degree of blue-shift and attenuation is closely related to the AuNP size, aggregation morphology, and PNB size. However, previous studies have mainly focused on the initial stages of PNB formation around AuNP shown in Fig. 1a-b. Few studies have been done on the effect of AuNP aggregation on the radiative properties and the influencing factors during AuNP aggregation, and PNB dissipation.

In the current study, the effect of AuNP aggregation on the radiation properties during light-induced vaporization process has been investigated based on the finite element modeling (FEM). Specifically, the influence of the number and morphology of AuNP aggregates on the radiation properties is studied.

2. Numerical Method and FEM Model

2.1 Radiative properties of an individual AuNP

The Mie scattering theory is considered the most precise approach for figuring out the radiative properties of nanospheres by solving Maxwell's equation [18]. In the presence of complicated geometrical structures composed of AuNP and PNB, however, a high-precision numerical method based on FEM was used to obtain the radiative properties of AuNPs [19, 20].

Under the LSPR effect, a maximum of light energy is converted into heat. Poynting's theorem states that this generated energy can be written as [6]:

$$Q = \iiint q dV = \iiint \frac{1}{2} \text{Re}(\mathbf{J} \cdot \sigma \mathbf{E}) dV \quad (1)$$

where q is the electromagnetic power loss density within the nanostructure integrated over the NP volume and \mathbf{J} is the current density. By utilizing FEM to numerically solve Maxwell's equation, one can determine \mathbf{E} , which is the electric field inside the nanostructure [19].

$$\nabla \times \mu_r^{-1} [\nabla \times \mathbf{E}(r)] - k_0^2 \left(\varepsilon_r - j \frac{\sigma}{\omega_0 \varepsilon_0} \right) \mathbf{E}(r) = 0 \quad (2)$$

where μ_r is the relative magnetic permeability, ω_0 is the angular frequency, ε_r is the frequency-dependent relative permittivities, $\varepsilon_r = (n - ik)^2$, n and k are the real and imaginary parts of the complex refractive index. σ is the electrical conductivity. $k_0 = 2\pi/\lambda$ is the wavenumber and λ is the wavelength.

The absorption cross sections of nanoparticles characterize their absorption properties of light as a function of wavelength. Dividing the rate of absorbed energy by the intensity of incident light gives an expression for the optical absorption cross section.

$$C_{\text{abs}} = \frac{1}{I_0} \iiint Q dV \quad (3)$$

The scattering cross section can be defined as:

$$C_{\text{sc}} = \frac{1}{I_0} \iint (\mathbf{n} \cdot \mathbf{S}_{\text{sc}}) dS \quad (4)$$

Where \mathbf{n} is the normal vector pointing outward from the nanoparticle, \mathbf{S}_{sc} is the scattering intensity (Poynting) vector, I_0 is the intensity of incident light. The integration is performed over the closed surface of the nanoparticle.

The extinction cross section of the nanoparticle is the sum of the above two cross sections.

$$C_{\text{ext}} = C_{\text{abs}} + C_{\text{sc}} \quad (5)$$

Because the PNB just scatters the incident light rather than absorbing it, the extinction cross section of the PNB, $C_{\text{ext-B}}$, can be expressed as:

$$C_{\text{ext-B}} = C_{\text{abs-B}} + C_{\text{sc-B}} = C_{\text{sc-B}} \quad (6)$$

Thus, the extinction cross section of the P-B complexes, $C_{\text{ext-C}}$, is the sum of the scattering cross section of the particles, $C_{\text{ext-P}}$, and the scattering cross section of PNB, $C_{\text{ext-B}}$, when PNBs are generated around the nanoparticles.

$$C_{\text{ext-C}} = C_{\text{ext-P}} + C_{\text{ext-B}} \quad (7)$$

Additionally, the spectral scattering albedo, ω , was used to measure the scattered energy as a proportion of the incident radiant energy for the entire wavelength band [21]. Albedo is the amount of energy reflected by the P-B complexes without being absorbed.

$$\omega = \frac{C_{\text{sc-B}}}{C_{\text{ext-C}}} = \frac{C_{\text{sc-P}} + C_{\text{sc-B}}}{C_{\text{ext-P}} + C_{\text{ext-B}}} \quad (8)$$

2.2 Simulation methods

In this work, we set different geometries into the finite element method (FEM) simulation software COMSOL Multiphysics and use the trial version to solve Maxwell's equations. Specifically, the incident light is incident from top to bottom along the z-axis and polarized along the x-axis. The water boundary is controlled by periodic boundary conditions, and the meshes are controlled by the physical field since the software can find the best grid distributions based on the geometry and input parameters. Absorbing boundaries, or perfectly matched layers (PMLs) are used to terminate the computing domain and prevent incident electromagnetic waves from reflecting at the boundaries. The optical constant of AuNP is obtained from Johnson's results [22]. The parametric scans are separated at 1 nm in the LSPR wavelength range and 10 nm in the remaining wavelength range to get the precise LSPR peak wavelength and shorten the computation time.

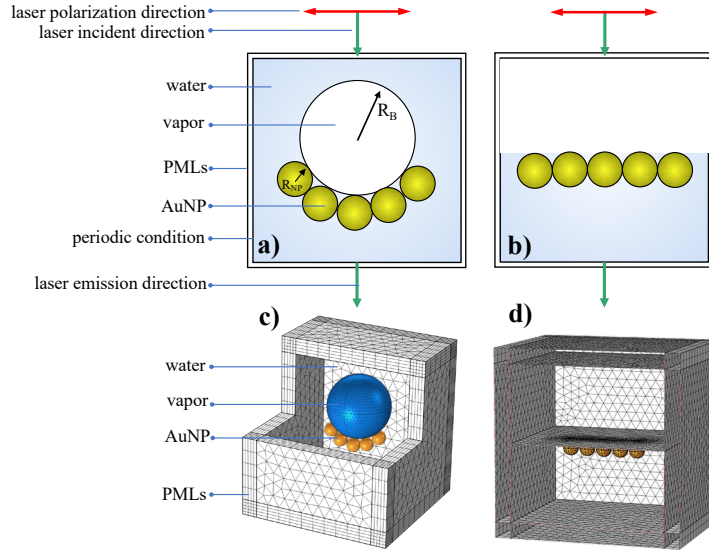


Fig. 2: Schematic diagram of the FEM computational model for the radiative properties. (a) Aggregation of AuNPs at the PNB boundary. (b) Aggregation of AuNPs on the liquid surface after PNB dissipation. (c-d) Meshes corresponding to the FEM model.

3. Results and Discussion

3.1 Effect of the aggregated number of AuNPs on the radiative properties of P-B complexes

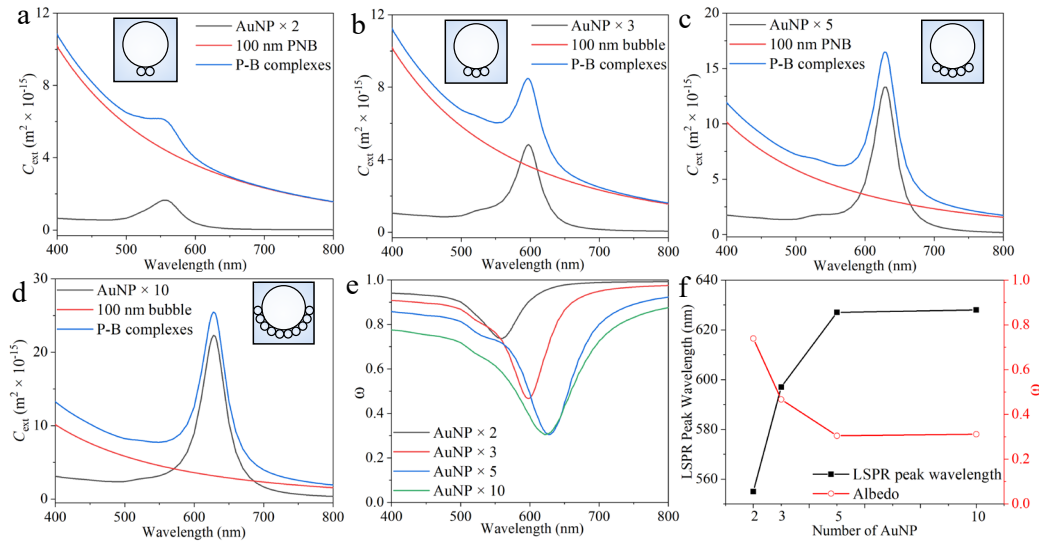


Fig. 3: Radiative properties of P-B complexes formed by attracting AuNPs with a radius of 10 nm around a PNB with a radius of 100 nm. (a-d) Extinction cross sections of AuNP aggregates, PNB, and P-B complexes after attracting different numbers of AuNPs around a PNB. The illustration is the schematic diagram of the corresponding calculation model. Dependence of the (e) albedo and (f) LSPR peak wavelength and albedo of P-B complexes on the number of aggregated AuNPs.

In Figs. 3a-d, a model of a PNB with a radius of 100 nm surrounded by aggregated AuNPs with a radius of 10 nm is presented to determine the effect of different numbers of aggregated AuNPs (2, 3, 5, and 10) on the radiative properties of P-B complexes. When the number of aggregated AuNPs reaches 3, the extinction effect of AuNP aggregates exceeds that of PNB, and the extinction effect of aggregates gradually dominates with the increase in the number of aggregated AuNPs. According to Figs. 3e and 3f, as the number of aggregated AuNPs rises, the LSPR peak wavelength of AuNP aggregates

dramatically shifts red, but when the number of aggregated AuNPs increases from 5 to 10, the LSPR peak wavelength remains almost unaltered. But the albedo of P-B complexes gradually decreases and is lower than 0.5 when the number of aggregated AuNPs reaches 3, indicating that the main contribution to the extinction effect of incident light by P-B complexes gradually changes from the scattering effect by AuNP aggregates and PNB to the absorption effect by AuNP aggregates during the aggregation of AuNPs induced by PNB.

3.2 Effect of aggregation morphology of AuNPs on the radiative properties of P-B complexes

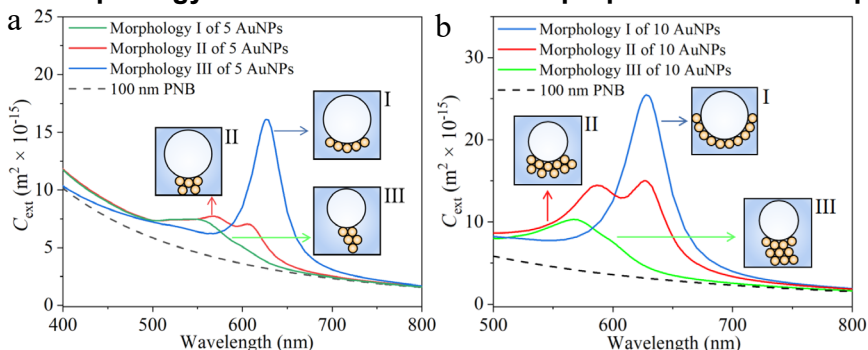


Fig. 4: Effect of the number of AuNP aggregation layers on the radiative properties of P-B complexes when (a) 5 and (b) 10 AuNPs with a radius of 10 nm are attracted around a 100 nm radius PNB.

In fact, AuNPs may be unevenly distributed in a string on the PNB spherical surface, they may be distributed in a two-dimensional structure on the PNB spherical surface, or even a few AuNPs may be dispersed on the periphery of the first layer of AuNPs, showing a three-dimensional structure. A model of 5 (Fig. 4a) and 10 (Fig. 4b) aggregated AuNPs around a PNB is constructed to compare the extinction properties of P-B complexes when one layer (aggregation form I), two layers (form II) and three layers (form III) of AuNPs are formed around a PNB. Fig. 4 makes it clear that the aggregation morphology of AuNPs affects their extinction properties in a significant way. In particular, as the number of aggregated layers of AuNPs increases, the extinction cross section of P-B complexes gradually decreases, and the LSPR peak wavelength is blue-shifted. Notably, two distinct absorption peaks are observed when AuNPs are aggregated in two layers outside the PNB.

3.3 Evolution of the radiative properties of AuNP aggregates after PNB dissipation

The insets in Fig. 5a is the FEM model of the radiative properties of AuNP aggregates on the fluid surface after PNB dissipation. The effect of the number of aggregated AuNPs (2, 3, 5, and 10) with a radius of 10 nm on the radiative properties of AuNP aggregates is investigated. As shown in Figs. 5a-d, the peak extinction cross section of AuNP aggregates increases and shows a linear relationship with the increase of the number of aggregated AuNPs. The LSPR peak wavelength of AuNP aggregates is considerably red-shifted, but when the number of aggregated AuNPs increases from 5 to 10, the increase in the LSPR peak wavelength is not obvious. The albedo of AuNP aggregates increases and shows a linear relationship with the increasing number of aggregated AuNPs, but the albedo does not exceed 0.5, indicating that the extinction effect is mainly dependent on the absorption effect of the AuNP aggregates. Similar to the previous section, the model of 5 (Fig. 5e) and 10 (Fig. 5f) AuNPs aggregated on the nanofluid surface is constructed to compare the extinction properties of AuNP aggregates when one layer (form I), two layers (form II) and three layers (form III) of AuNPs are formed on the fluid surface. It can be found that the extinction cross section of AuNP aggregates gradually decreases and the LSPR peak wavelength of AuNP aggregates is blue-shifted as the aggregated layer of AuNPs increases. Notably, two distinct absorption peaks appear when 10 AuNPs are aggregated into two layers on the nanofluid surface. In addition, when AuNPs are aggregated into multiple layers, the alignment direction of AuNP aggregates is often not parallel to the polarization direction of the incident light, but shows a certain offset angle. Due to an obvious shadowing effect of the upper AuNP on the lower one [23], the radiation properties of AuNP aggregates will be attenuated.

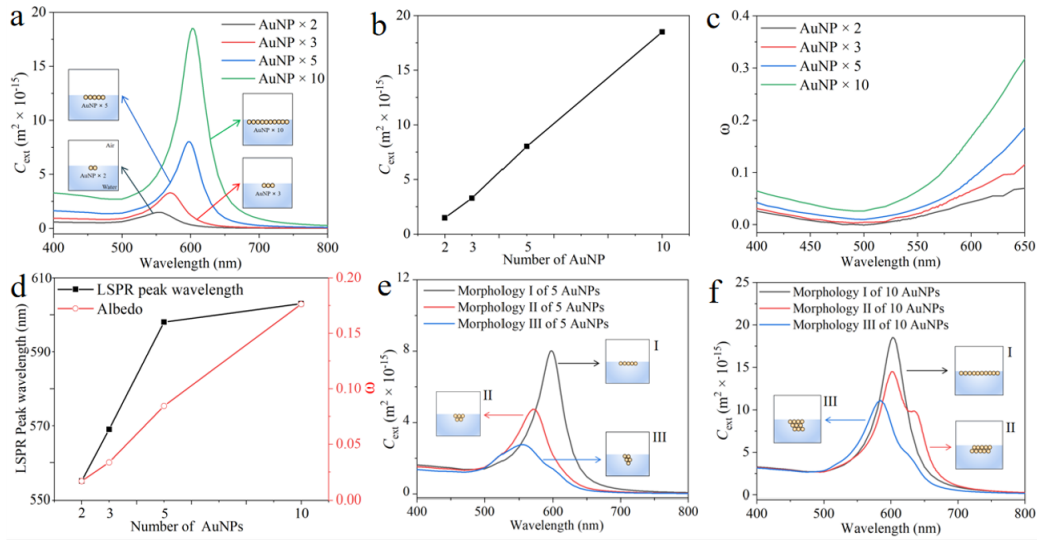


Fig. 5: Radiative properties of aggregates formed by AuNPs with a radius of 10 nm on the fluid surface after PNB dissipation. Dependence of (a) extinction cross section (b) peak extinction cross section (c) albedo (d) LSPR peak wavelength and albedo at LSPR peak wavelength of AuNP aggregates on the number of aggregated AuNPs. (e-f) Effect of aggregation morphology on the extinction properties of AuNP aggregates.

3.4 Evolution of radiative properties during light-induced vaporization process of nanofluid

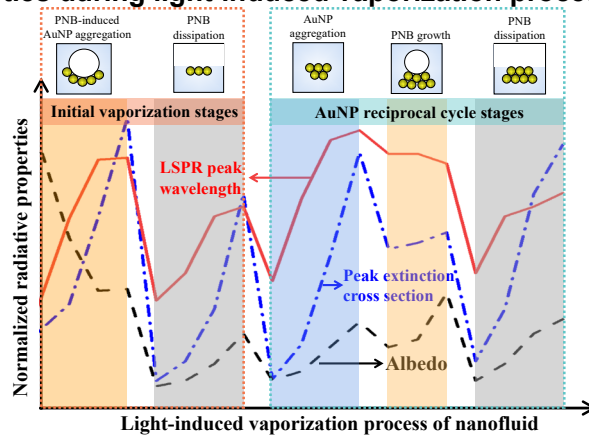


Fig. 6: Non-linear evolution of radiative properties during light-induced vaporization process of nanofluid.

As shown in Fig. 6, it is evident that the radiative properties (LSPR peak wavelength, peak extinction cross section, and albedo at LSPR peak wavelength) exhibit obvious non-linear evolution rules on the time scale. In addition, the AuNP aggregates continuously and repeatedly move in the fluid under the effect of the PNBs' buoyancy force, making the radiative properties of the nanofluid show a periodic evolution pattern until the fluid is completely evaporated. Certainly, the reciprocal cycle motion law of nanoparticles is more complex and may exist only locally in the fluid, which has been preliminarily confirmed by the experiments of Domínguez-Juárez et al[24].

Specifically, during the PNB-induced aggregation stage of AuNPs, with the increase in the number of aggregated AuNPs, the peak extinction cross section noticeably increases. The reduction in albedo suggests that the absorption of incident light by AuNP aggregates gradually increases. After PNB dissipation, the peak extinction cross section of AuNP aggregates increased continuously as the number of aggregated AuNPs increased, and the LSPR peak wavelength is red-shifted; however, the effect of red-shift is not apparent once the number of aggregated AuNPs increases to a certain degree. The albedo rises but is still low, showing that the extinction effect is mostly dependent on the absorption of light energy by

AuNP aggregates. In the subsequent reciprocal cycle stages, with the increase in the number of aggregated AuNPs, the LSPR peak wavelength of AuNP aggregates is red-shifted, the peak extinction cross section progressively rises, and the albedo gradually rises but remains low. When PNBs generate around AuNP aggregates, the LSPR peak wavelength of AuNP aggregates is slightly blue-shifted, the extinction peak and albedo of P-B complexes gradually increase. When PNBs dissipate, the number of aggregated AuNPs increases significantly compared with the PNB dissipation phase in the initial vaporization stages, and the variation trend of the radiative properties of AuNP aggregates in the AuNP reciprocal cycle stages is similar to that of the PNB dissipation process in the initial vaporization stage, but the degree of increase in radiation properties is stronger in comparison to the initial vaporization stages. After the completely evaporation of the fluid, the variation of the radiative properties is closely related to the morphology of the AuNP aggregates.

4. Conclusion

A FEM calculation model of the radiative properties during light-induced vaporization of nanofluid is built to investigate the effect of AuNP aggregation process on the radiative properties of P-B complexes. According to numerical calculations, the radiative properties exhibit an obvious non-linear evolution law on the time scale and a periodic evolution pattern in the reciprocal cycle stages. The following conclusions can be derived from the calculations of radiative properties:

1. The aggregation of AuNPs causes a red-shift in the peak LSPR wavelength of AuNP aggregates, while the generation of PNB causes a blue-shift in the peak LSPR wavelength of AuNPs. In the presence of PNB, the change in the peak LSPR wavelength of P-B complexes depends on the competition between the red-shift effect of AuNPs aggregation and the blue-shift effect of PNB, but in general the red-shifting effect of AuNP aggregation is stronger than the blue-shifting effect of PNB growth.

2. The aggregation of AuNPs contributes to the increase in the peak extinction cross section of P-B complexes.

3. The albedo of P-B complexes above 0.5 implies that the scattering effect of AuNPs and PNBs on incident light exceeds the absorption effect of AuNPs. In the presence of PNB, whether the albedo of P-B complexes exceeds 0.5 depends on the relative magnitude of the extinction cross section of AuNP aggregates and PNB. After the dissipation of PNBs, only the scattering effect of AuNP aggregates on the incident light exists, and the aggregation of AuNPs increases the albedo of AuNP aggregates, although at this point it is lower (below 0.5) compared to that in the presence of PNB, showing a strong absorption of incident light.

4. The aggregation morphology of AuNPs greatly impacts the radiative properties of the aggregates, which is shown by the reduced peak extinction cross section, the blue-shifted LSPR peak wavelength of AuNP aggregates, the increase in the LSPR peak width, and the potential for multiple extinction peaks with the increase in the number of aggregation layers.

The results of this study not only show the influence of AuNP aggregation on the radiation properties, but also reveal the non-linear evolution of radiation properties during the vaporization process of nanofluid. The changes in radiation properties have an impact on the absorption of light source energy by AuNPs, which in turn influences the heat transfer inside the nanofluid. Ultimately, this will affect the generation and evolution of PNB. The whole process is interconnected and is the fundamental reason for the non-linear changes in the radiation properties of nanofluid under light illumination. The results of this study will be helpful to develop and optimize the plasmonic-enhanced applications of bubbles in emerging fields, ranging from optofluidic control, microscale/nanoscale manipulation to biomedicine.

Acknowledgements

The support of this work by the Natural Science Foundation of Shanghai (No. 20ZR1459600) and the Fundamental Research Funds for the Central Universities of China is gratefully acknowledged.

References

- [1] C. Zhao, W. An, Y. Zhang, Q. Dong and N. Gao, "Impact of enhanced electric field on light-induced evaporation process of plasmonic nanofluid," *Int. J. Heat Mass Transf.*, vol. 189, pp. 122708, 2022.
- [2] Neumann, A. S. Urban, J. K. Day, S. Lal, P. J. Nordlander and N. J. Halas, "Solar vapor generation enabled by nanoparticles," *ACS Nano*, vol. 7, pp. 42-49, 2013.
- [3] W. An, Y. Zhang, B. Pang and J. Wu, "Synergistic design of an integrated pv/distillation solar system based on nanofluid

spectral splitting technique,” *AIMS Energy*, 2021;9:534-57. vol. 9, no. 3, pp. 534-557, 2022.

- [4] K. Zhang, A. Jian, X. Zhang, Y. Wang, Z. Li and H. Y. Tam, “Laser-induced thermal bubbles for microfluidic applications,” *Lab Chip*, vol. 11, pp. 1389-1395, 2011.
- [5] A. Shakeri-Zadeh, H. Zareyi, R. Sheervalilou, S. Laurent, H. Ghaznavi and H. Samadian, “Gold nanoparticle-mediated bubbles in cancer nanotechnology,” *J. Control. Release*, vol. 330, pp. 49-60, 2021.
- [6] L. Jauffred, A. Samadi, H. Klingberg, P. M. Bendix and L. B. Oddershede, “Plasmonic heating of nanostructures,” *Chem. Rev.*, vol. 119, pp. 8087-8130, 2019.
- [7] E. Lukianova-Hleb, Y. Hu, L. Latterini, L. Tarpani, S. Lee, R. A. Drezek, J. H. Hafner, and D. O. Lapotko, “Plasmonic nanobubbles as transient vapor nanobubbles generated around plasmonic nanoparticles,” *ACS Nano*, vol. 4, pp. 2109-2123, 2010.
- [8] K. Sasikumar and P. Koblinski, “Molecular dynamics investigation of nanoscale cavitation dynamics,” *J. Chem. Phys.*, vol. 141, pp. 234508, 2014.
- [9] T. Katayama, K. Setoura, D. Werner, H. Miyasaka and S. Hashimoto, “Picosecond-to-nanosecond dynamics of plasmonic nanobubbles from pump-probe spectral measurements of aqueous colloidal gold nanoparticles,” *Langmuir*, vol. 30, pp. 9504-9513, 2014.
- [10] C. Zhao, Y. Xie, Z. Mao, Y. Zhao, J. Rufo, S. Yang, F. Guo, J. D. Mai, and T. J. Huang, “Theory and experiment on particle trapping and manipulation via optothermally generated bubbles,” *Lab Chip*, vol. 14, no. 2, pp. 384-391, 2014.
- [11] H. Takeuchi, M. Motosuke and S. Honami, “Noncontact bubble manipulation in microchannel by using photothermal marangoni effect,” *Heat Transfer Eng.*, vol. 33, no. 3, pp. 234-244, 2012.
- [12] J. Neumann and R. Brinkmann, “Self-limited growth of laser-induced vapor bubbles around single microabsorbers,” *Appl. Phys. Lett.*, vol. 93, pp. 033901, 2008.
- [13] J. Neumann and R. Brinkmann, “Nucleation dynamics around single microabsorbers in water heated by nanosecond laser irradiation,” *J. Appl. Phys.*, vol. 101, pp. 114701, 2007.
- [14] G. Baffou, J. Polleux, H. Rigneault and S. Monneret, “Super-heating and micro-bubble generation around plasmonic nanoparticles under cw illumination,” *J. Phys. Chem. C*, vol. 118, pp. 4890-4898, 2014.
- [15] Z. Fang, Y. R. Zhen, O. Neumann, A. Polman, F. J. Garcia de Abajo, P. Nordlander and N. J. Halas, “Evolution of light-induced vapor generation at a liquid-immersed metallic nanoparticle,” *Nano Lett.*, vol. 13, no. 4, pp. 1736-42, 2013.
- [16] V. Kotaidis and A. Plech, “Cavitation dynamics on the nanoscale,” *Appl. Phys. Lett.*, vol. 87, pp. 213102, 2005.
- [17] K. Setoura, D. Werner and S. Hashimoto, “Optical scattering spectral thermometry and refractometry of a single gold nanoparticle under cw laser excitation,” *J. Phys. Chem. C*, vol. 116, pp. 15458-15466, 2012.
- [18] R. Yang, D. Li, W. Wei and F. Wang. “A Mie optimization model to determine optical properties of PCM based nanofluids for solar thermal applications of glazing window,” *Optik*, vol. 212, pp. 164664, 2020.
- [19] J. Zhao, A. O. Pinchuk, J. M. McMahon, S. Li, L. K. Ausman, A. L. Atkinson and G. C. Schatz, “Methods for describing the electromagnetic properties of silver and gold nanoparticles,” *Acc. Chem. Res.*, vol. 41, no. 12, pp. 1710-1720, 2008.
- [20] J. Parsons, C.P. Burrows, J.R. Sambles and W.L. Barnes, “A comparison of techniques used to simulate the scattering of electromagnetic radiation by metallic nanostructures,” *J. Mod. Optic.*, vol. 57, no. 5, pp. 356-365, 2010.
- [21] K. Liu, X. Xue and E. P. Furlani, “Theoretical comparison of optical properties of near-infrared colloidal plasmonic nanoparticles,” *Sci. Rep.*, vol. 6, pp. 34189, 2016.
- [22] P. B. Johnson and R. W. Christy, “Optical constants of the noble metals,” *Phys. Rev. B*, vol. 6, pp. 4370-4379, 1972.
- [23] G. Baffou, R. Quidant and F. J. García de Abajo, “Nanoscale control of optical heating in complex plasmonic systems,” *ACS Nano*, vol. 4, no. 2, pp. 709-716, 2010.
- [24] J. L. Domínguez-Juárez, S. Vallone, A. Lempel, M. Moocarme, J. Oh, H. D. Gafney and L. T. Vuong, “Influence of solvent polarity on light-induced thermal cycles in plasmonic nanofluids,” *Optica*, vol. 2, no. 5, pp. 447-453, 2015.